Crystallization and preliminary X-ray diffraction analyses of the TIR domains of three TIR–NB–LRR proteins that are involved in disease resistance in *Arabidopsis thaliana*

Li Wan,[a]‡ Xiaoxiao Zhang,[a]‡ Simon J. Williams,[a]‡ Thomas Ve,[a] Maud Bernoux,[b] Kee Hoon Sohn,[c] Jonathan D. G. Jones,[c] Peter N. Dodds[b] and Bostjan Kobe[a]*

[a]School of Chemistry and Molecular Biosciences, Institute for Molecular Bioscience (Division of Chemistry and Structural Biology) and Australian Infectious Diseases Research Centre, University of Queensland, Brisbane, QLD 4072, Australia, [b]CSIRO Plant Industry, Canberra, ACT 2601, Australia, and [c]The Sainsbury Laboratory, Norwich Research Park, Norwich NR4 7UH, England

‡ These authors contributed equally to this work.

Correspondence e-mail: b.kobe@uq.edu.au

The Toll/interleukin-1 receptor (TIR) domain is a protein–protein interaction domain that is found in both animal and plant immune receptors. The N-terminal TIR domain from the nucleotide-binding (NB)–leucine-rich repeat (LRR) class of plant disease-resistance (R) proteins has been shown to play an important role in defence signalling. Recently, the crystal structure of the TIR domain from flax R protein L6 was determined and this structure, combined with functional studies, demonstrated that TIR-domain homodimerization is a requirement for function of the R protein L6. To advance the molecular understanding of the function of TIR domains in R-protein signalling, the protein expression, purification, crystallization and X-ray diffraction analyses of the TIR domains of the *Arabidopsis thaliana* R proteins RPS4 (resistance to *Pseudomonas syringae* 4) and RRS1 (resistance to *Ralstonia solanacearum* 1) and the resistance-like protein SNC1 (suppressor of *npr1-1*, constitutive 1) are reported here. RPS4 and RRS1 function cooperatively as a dual resistance-protein system that prevents infection by three distinct pathogens. SNC1 is implicated in resistance pathways in *Arabidopsis* and is believed to be involved in transcriptional regulation through its interaction with the transcriptional corepressor TPR1 (Topless-related 1). The TIR domains of all three proteins have successfully been expressed and purified as soluble proteins in *Escherichia coli*. Plate-like crystals of the RPS4 TIR domain were obtained using PEG 3350 as a precipitant; they diffracted X-rays to 2.05 Å resolution, had the symmetry of space group $P1$ and analysis of the Matthews coefficient suggested that there were four molecules per asymmetric unit. Tetragonal crystals of the RRS1 TIR domain were obtained using ammonium sulfate as a precipitant; they diffracted X-rays to 1.75 Å resolution, had the symmetry of space group $P4_12_12$ or $P4_32_12$ and were most likely to contain one molecule per asymmetric unit. Crystals of the SNC1 TIR domain were obtained using PEG 3350 as a precipitant; they diffracted X-rays to 2.20 Å resolution and had the symmetry of space group $P4_12_12$ or $P4_32_12$, with two molecules predicted per asymmetric unit. These results provide a good foundation to advance the molecular and structural understanding of the function of the TIR domain in plant innate immunity.

1. Introduction

Plants have developed a complex multilayered immune system to defend themselves against invading pathogens (Jones & Dangl, 2006). The first basal layer of immunity is termed PAMP (pathogen-associated molecular pattern)-triggered immunity (PTI) and involves the recognition of conserved PAMPs by pattern-recognition receptors (PRRs) on the exterior surface of the plant cell. The second layer involves the recognition of pathogen effector proteins by intracellular disease-resistance (R) proteins and is named effector-triggered immunity (ETI). ETI is often mediated by R proteins from the nucleotide-binding (NB) and leucine-rich repeat (LRR) class, which directly or indirectly recognize pathogen effector proteins. Once activated, NB–LRR proteins trigger defence responses that are often associated with localized cell death at infection sites through a process known as the hypersensitive response (HR; Chisholm *et al.*, 2006). NB–LRR R proteins have either a coiled-coil (CC) or Toll/interleukin-1 receptor (TIR) domain at their amino-termini and are therefore grouped as CNL and TNL R proteins, respectively (Dodds & Rathjen, 2010). The central NB domain is believed to act as a
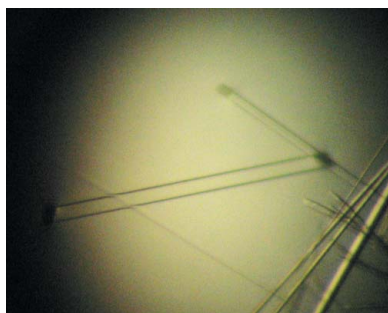
Table 1
Crystallographic data collection and processing.

Values in parentheses are for the outer shell.

	RPS4	RRS1 data set 1	RRS1 data set 2	SNC1
Detector	ADSC Quantum 315r CCD	ADSC Quantum 315r CCD	ADSC Quantum 315r CCD	ADSC Quantum 315r CCD
Wavelength (Å)	0.9537	0.9537	1.3776	0.9537
Temperature (K)	100	100	100	100
Crystal-to-detector distance (mm)	320	180	170	310
Rotation range per image (°)	1	1	1	0.5
Exposure time per image (s)	1	1	1	1
Space group	$P1$	$P4_12_12$ or $P4_32_12$	$P4_12_12$ or $P4_32_12$	$P4_12_12$ or $P4_32_12$
Unit-cell parameters				
a (Å)	33.92	71.26	71.38	82.18
b (Å)	78.64	71.26	71.38	82.18
c (Å)	80.67	66.72	66.90	124.1
α (°)	65.63	90.00	90.00	90.00
β (°)	78.64	90.00	90.00	90.00
γ (°)	78.93	90.00	90.00	90.00
Average mosaicity† (°)	0.20	0.16	0.15	0.15
Resolution range (Å)	19.6–2.05 (2.11–2.05)	71.24–1.75 (1.78–1.75)	71.38–2.00 (2.11–2.00)	19.68–2.20 (2.27–2.20)
Total No. of reflections	165463 (10611)	251704 (10757)	929431 (130931)	372024 (32369)
No. of unique reflections	43623 (2762)	17927 (955)	12244 (1735)	22223 (1888)
Completeness (%)	94.0 (75.3)	100.0 (100.0)	100.0 (99.8)	99.8 (99.6)
Multiplicity†	3.8 (3.8)	14.0 (11.3)	75.9 (75.5)	16.7 (17.1)
Mean $I/\sigma(I)$	16.0 (5.9)	32.3 (1.7)	61.7 (11.5)	17.8 (2.1)
R_{meas}‡ (%)	7.0 (27.3)	7.0 (167.3)	7.0 (64.3)	18.0 (184.9)
$R_{p.i.m.}$§ (%)	3.6 (13.9)	1.9 (49.4)	0.8 (7.3)	4.3 (44.1)
$CC_{1/2}$¶	0.99 (0.95)	0.99 (0.59)	0.99 (0.98)	0.99 (0.69)
Matthews coefficient†† (Å³ Da⁻¹)	2.44	2.49	2.51	2.63
DelAnom correlation between half sets†			0.43 (0.03)	

† Calculated with *AIMLESS* (Evans & Murshudov, 2013) within the *CCP*4 suite (Winn *et al.*, 2011). ‡ $R_{meas} = \sum_{hkl}\{N(hkl)/[N(hkl)-1]\}^{1/2}\sum_i |I_i(hkl) - \langle I(hkl)\rangle|/\sum_{hkl}\sum_i I_i(hkl)$, where $I_i(hkl)$ is the intensity of the ith measurement of an equivalent reflection with indices hkl. § $R_{p.i.m.} = \sum_{hkl}\{1/[N(hkl)-1]\}^{1/2}\sum_i |I_i(hkl) - \langle I(hkl)\rangle|/\sum_{hkl}\sum_i I_i(hkl)$. ¶ Pearson correlation coefficient between independently merged halves of the data set, as defined by Karplus & Diederichs (2012) and calculated with *AIMLESS* (Evans & Murshudov, 2013) within the *CCP*4 suite (Winn *et al.*, 2011). †† Calculated with *MATTHEWS_COEF* (Kantardjieff & Rupp, 2003; Matthews, 1968) within the *CCP*4 suite (Winn *et al.*, 2011); corresponding to the most likely number of molecules in the asymmetric unit.

molecular switch, utilizing the exchange of ADP and ATP to control activity (Lukasik & Takken, 2009; Williams *et al.*, 2011), while the LRR domain has been shown to determine recognition specificity (Dodds *et al.*, 2006; Padmanabhan *et al.*, 2009; Ravensdale *et al.*, 2012; Wang *et al.*, 2007).

The N-terminal CC and TIR domains are believed to be involved in R-protein signalling. Recent reports of the crystal structures of the CC domain of the barley R protein MLA10 (Maekawa *et al.*, 2011) and the TIR domain of the flax R protein L6 (Bernoux *et al.*, 2011) helped to confirm this role. Maekawa and coworkers demonstrated that the CC domain of MLA10 forms a homodimer and mutational studies showed that this property is required for defence signalling (Maekawa *et al.*, 2011). Similarly, the TIR domain of L6 has the capacity to homodimerize. Crystallographic and mutational studies identified a dimerization interface and a signalling interface in this domain. The TIR domain of L6 is also required and sufficient to induce cell death (Bernoux *et al.*, 2011).

In *Arabidopsis*, RPS4 and RRS1 have been shown to cooperatively confer resistance to both fungal and bacterial pathogens (*Colletotrichum higginsianum*, *Ralstonia solanacearum* and *Pseudomonas syringae* pv. *tomato* strain DC3000 expressing *avrRps4*; Narusaka, Kubo *et al.*, 2009; Narusaka, Shirasu *et al.*, 2009; Birker *et al.*, 2009). Several examples of paired NB–LRR genes acting cooperatively to confer resistance against a pathogen have been reported (Ashikawa *et al.*, 2008; Lee *et al.*, 2009; Sinapidou *et al.*, 2004; Okuyama *et al.*, 2011; Yuan *et al.*, 2011). Both RPS4 and RRS1 belong to the TNL class of R proteins (Deslandes *et al.*, 2002; Gassmann *et al.*, 1999). Interestingly, RRS1 carries an additional C-terminal WRKY DNA-binding domain. RRS1 has been found to localize to the nucleus (Deslandes *et al.*, 2003), while RPS4 is distributed both in the nucleus and cytoplasm, but nuclear localization is required for full pathogen resistance (Wirthmueller *et al.*, 2007). While the genetic link between

RPS4 and RRS1 in this cooperative dual-function resistance has been established, the molecular basis of this cooperation is largely unknown.

A mutation in the *A. thaliana* NB–LRR R-like protein-encoding gene *SNC1* (suppressor of *npr1-1*, constitutive 1) leads to an auto-active phenotype (constitutive expression of defence genes and enhanced disease resistance against the virulent bacterial pathogen *Pseudomonas syringae* pv. *maculicola* ES4326 and the oomycete pathogen *Hyaloperonospora arabidopsidis* Noco2; Li *et al.*, 2001). SNC1 has been reported to function through an association with the transcriptional corepressor protein Topless-related 1 (TPR1; Zhu *et al.*, 2010). Overexpression of TPR1 activates SNC1-mediated immune responses, and GST pull-down assays have demonstrated that TPR1 associates with the SNC1 TIR domain *in vitro* (Zhu *et al.*, 2010). However, the molecular basis of these associations remains unknown.

As a step towards further elucidating the mechanisms involved in R-protein signalling, we report the expression, purification and crystallization studies of the TIR domains of the *A. thaliana* proteins RPS4, RRS1 and SNC1. Because RPS4 and RRS1 function as a dual resistance-protein system, the study should reveal interesting differences in the molecular mechanism of TIR-domain signalling compared with the L6 protein. Comparative studies of different R-protein TIR domains will further shed light on the common features of the interfaces involved in TIR–TIR domain interactions.
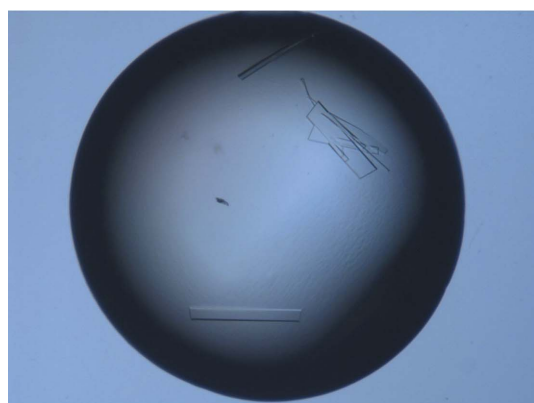
2. Materials and methods

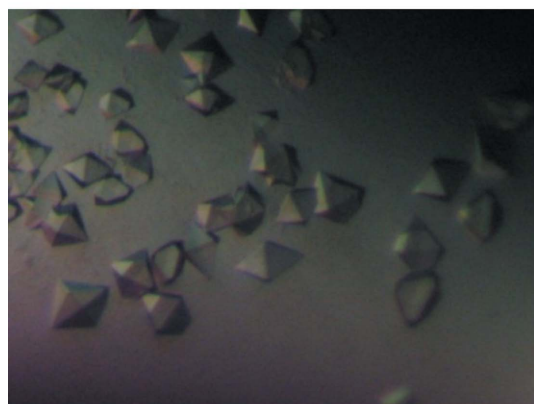### 2.1. Protein production and purification

The cDNAs comprising the TIR domains, encoding residues 6–153 of RRS1 (designated RRS1TIR) and 10–178 of RPS4 (designated

RPS4TIR), were amplified by PCR and inserted into the pMCSG7 vector using ligation-independent cloning (Stols *et al.*, 2002) using the following primer combinations (RRS1[6FW], 5′-TACTTCCAATCCAAT-GCGAAGGATGAGGAATTCGTGTGCATCAGCTGCGTAG-3′; RRS1[153RV], 5′-TATTCCACTTCCAATGTTATCCAATTCGTCCAA-CATAAAAGTGCGTCTCGTACACATC-3′; RPS4[10FW], 5′-TACTTC-CAATCCAATGCGGAAGACAAGCCACCGCAGCATCAGGTG-3′; RPS4[178RV], 5′-TTATCCACTTCCAATGTTATATTCCGGTCA-ACGCTGTCTTCACCGCC-3′). For SNC1, a synthetic gene, codon-
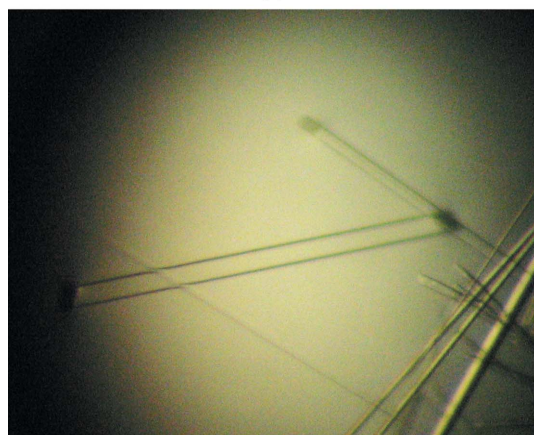
optimized for expression in *Escherichia coli*, that encoded residues 1–184 was purchased from GeneArt (Life Technologies). The cDNA for the TIR domain-encoding residues 8–181 of SNC1 (designated SNC1TIR) was amplified by PCR and inserted into the pMCSG7 vector using ligation-independent cloning (Stols *et al.*, 2002) using the primer combination SNC1[8FW], 5′-TACTTCCAATCCAATGCG-GGTAGCCGTCGTTATGATGTTTTTCCGAG-3′; SNC1[181RV], 5′-TATTCCACTTCCAATGTTAACCAAAATCATCACTCGGGG-TCATGGTTT-3′. The resulting constructs contained an N-terminal His$_6$ tag followed by a TEV (*Tobacco etch virus*) protease cleavage site. The integrity of the constructs was confirmed by sequencing. The expected molecular weights of RPS4TIR, RRS1TIR and SNC1TIR are 20, 17 and 19 kDa, respectively. The RRS1TIR and RPS4TIR constructs were expressed in *E. coli* Rosetta (DE3) cells, while SNC1TIR was expressed in *E. coli* BL21 (DE3) cells. For expression, the auto-induction method was used (Studier, 2005). In brief, cells were grown by continuous shaking at 310 K until the OD$_{600\,nm}$ reached 0.6–0.8. The temperature was then lowered to 293 K for RPS4TIR and SNC1TIR and to 288 K for RRS1TIR and the cells were grown for a further 18 h before harvesting by centrifugation. Cells expressing RPS4TIR and SNC1TIR were resuspended in lysis buffer consisting of 50 mM HEPES pH 8.0, 500 mM NaCl, 1 mM DTT, while the cells expressing the RRS1TIR domain were resus-pended in lysis buffer consisting of 50 mM HEPES pH 8.0, 150 mM NaCl, 1 mM DTT. The cells were lysed using sonication and were clarified by centrifugation (10 000g) for 40 min. The resulting super-natant was applied onto a 5 ml HisTrap column (GE Healthcare) pre-equilibrated with lysis buffer containing 30 mM imidazole. An ÄKTA FPLC system (GE Healthcare) was used for all chromatography steps. The column was washed with lysis buffer containing 30 mM imidazole to remove proteins interacting nonspecifically and the bound protein was eluted using a linear gradient of imidazole from 30 to 250 mM. Fractions containing the protein of interest, as deter-mined by Coomassie-stained SDS–PAGE, were pooled and buffer-exchanged into a TEV protease-compatible buffer (100 mM Tris pH 8.0, 250 mM NaCl, 1 mM DTT, 0.05 mM EDTA). The N-terminal His$_6$ tag was removed by overnight treatment with His$_6$-tagged TEV protease at 277 K (100 µg per 5 mg of the protein of interest). The cleaved protein was reapplied onto the HisTrap column (pre-equili-brated with lysis buffer containing 30 mM imidazole) to remove the TEV protease and other contaminants. Unbound material that contained the tag-cleaved protein of interest was collected, concen-trated and applied onto a Superdex 75 HiLoad 26/60 size-exclusion column (GE Healthcare) pre-equilibrated with gel-filtration buffer consisting of 10 mM HEPES pH 7.5, 150 mM NaCl, 1 mM DTT. The peak fractions were pooled and concentrated using Amicon Ultra-15 Centrifugal Filter Units (Millipore) to final concentrations of 10 mg ml^{-1} for RPS4TIR and SNC1TIR and 16 mg ml^{-1} for RRS1TIR. The purity of all of the purified proteins was estimated to be greater than 95% by Coomassie-stained SDS–PAGE. All proteins were stored in the gel-filtration buffer in aliquots at 193 K prior to setting up crystal trays.

2.2. Crystallization and X-ray data collection and processing

The optimal protein concentration for crystallization was deter-mined using the PCT screen (Hampton Research). Initial screening was conducted in 96-well plates (Labtech) at 293 K using the hanging-drop vapour-diffusion method. Eight commercial screens were utilized: Index, PEG/Ion and PEGRx (Hampton Research), Morpheus, ProPlex, JCSG *plus* and PACT *premier* (Molecular Dimensions) and Precipitant Synergy (Emerald BioSystems).

(a)

(b)

(c)

Figure 1
(*a*) Crystals of RPS4TIR grown after 1 d in 23%(*w/v*) PEG 3350, 0.2 *M* ammonium citrate pH 6.5, 0.2 *M* sodium chloride (approximate dimensions 150 × 150 × 10 µm). (*b*) Crystals of RRS1TIR grown after 1 d in 0.1 *M* bis-tris pH 7.0, 1.8 *M* ammonium sulfate (approximate dimensions 180 × 120 × 80 µm). (*c*) Crystals of SNC1TIR grown after 1 d in 18%(*w/v*) PEG 3350, 9%(*w/v*) glycerol, 0.1 *M* MMT buffer pH 7.5 (∼0.6 mm in the longest dimension).

crystallization communications

Hanging drops consisting of 100 nl protein solution and 100 nl reservoir solution were set up using a Mosquito robot (TTP LabTech, UK) and were equilibrated against 100 µl reservoir solution. The drops were monitored and imaged using a Rock Imager system (Formulatrix, USA).

Hits from the initial crystallization screens were optimized by varying the protein concentration, the precipitant concentration, the pH and the drop size and by using the Additive Screen (Hampton Research). Crystals were mounted in nylon loops and transferred into well solution containing 25%(v/v) glycerol as the final concentration prior to flash-cooling in liquid nitrogen.

For both RPS4TIR and SNC1TIR, an X-ray diffraction data set was collected from one single crystal in each case on the Australian Synchrotron MX2 beamline at a wavelength of 0.9537 Å (Table 1). Two data sets were collected for RRS1TIR at wavelengths of 0.9537 and 1.3776 Å (named data set 1 and 2, respectively) on the Australian Synchrotron MX2 beamline (Table 1). Data were collected using the *Blu-Ice* software (McPhillips *et al.*, 2002), indexed and integrated using *XDS* (Kabsch, 2010) and scaled with *AIMLESS* (Evans & Murshudov, 2013) within the *CCP*4 suite (Winn *et al.*, 2011).

3. Results and discussion

The domain boundaries of the expression constructs were selected based on sequence alignments of RPS4, RRS1 and SNC1 with TIR domains of known structure, including those from flax L6 protein (Bernoux *et al.*, 2011) and *Arabidopsis* NP_177436/At1g72930 (AtTIR; Chan *et al.*, 2010). The sequence identities of RPS4TIR, RRS1TIR and SNC1TIR to L6TIR are 28, 16 and 36%, respectively. The sequence identities of RPS4TIR, RRS1TIR and SNC1TIR to AtTIR are 32, 23 and 37%, respectively. Four truncated variants each of the RRS1 TIR domain (residues 1–148, 1–153, 6–148 and 6–153) and the RPS4 TIR domain (residues 1–178, 1–183, 10–183 and 10–178) were generated. For the RRS1 TIR domain, the RRS1[6–153] variant (comprising residues 6–153; referred to here as RRS1TIR) was chosen for further study because of the superior protein-expression levels achieved in *E. coli* and the higher purity obtained after purification. For the RPS4 TIR domain, all four variants were soluble and could be purified to homogeneity. Both the RPS4[1–183] and the RPS4[10–178] variants yielded crystals in sparse-matrix screens. However, the crystals formed by RPS4[10–178] (referred to here as RPS4TIR) proved easier to optimize and diffraction-quality crystals were obtained. For the SNC1 TIR domain, the SNC1[8–181] variant
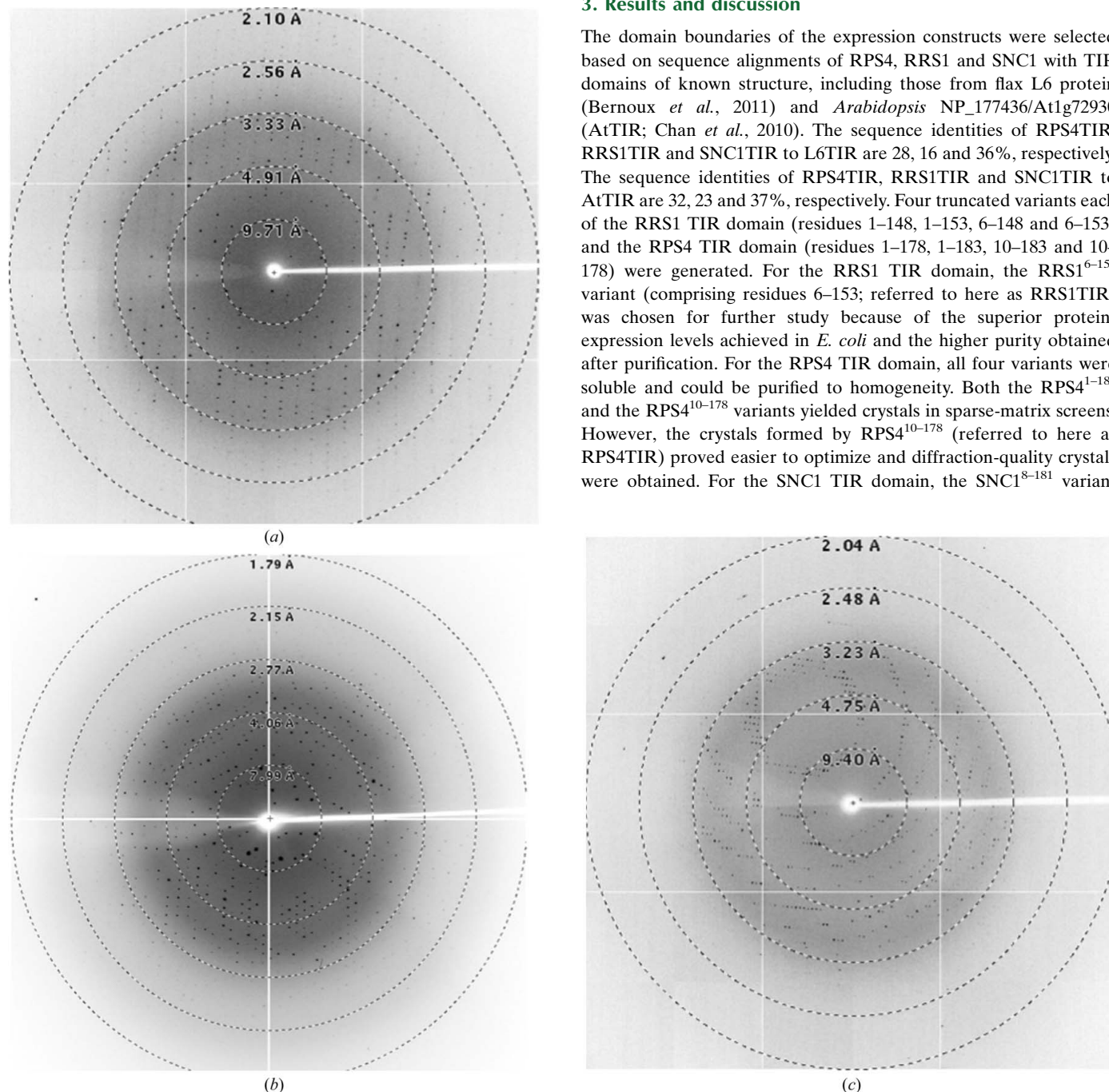

Figure 2
Diffraction images of RPS4TIR, RRS1TIR and SNC1TIR crystals. The X-ray diffraction images were collected on the MX2 beamline of the Australian Synchrotron (see §2 and Table 1 for details). (*a*) Diffraction image of the RPS4TIR crystal, (*b*) diffraction image of the RRS1TIR crystal (from data set 1), (*c*) diffraction image of the SNC1TIR crystal.
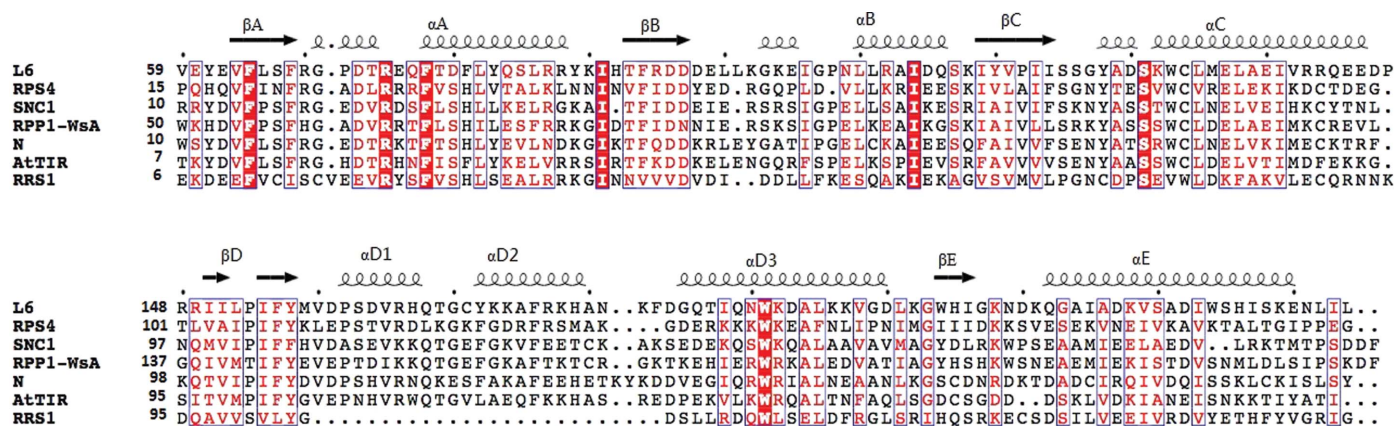
Figure 3
Multiple sequence alignment of TIR domains. Amino-acid sequences from the TIR domains of *Arabidopsis* RPS4 (residues 15–191), *Arabidopsis* SNC1 (10–180), *Arabidopsis* RPP1-WsA (50–229), tobacco N (10–191) and *Arabidopsis* RRS1 (6–153) were aligned with the sequences of TIR domains with known crystal structures, *Arabidopsis* AtTIR (PDB entry 3jrn; Chan *et al.*, 2010) and flax L6 (PDB entry 3ozi; Bernoux *et al.*, 2011), using *MUSCLE* (Edgar, 2004). The positions of the secondary-structure elements in L6 are shown at the top. The alignment was formatted using *ESPript* (Gouet *et al.*, 2003).

(referred to here as SNC1TIR) was studied and could be produced in a soluble form in *E. coli*.

The optimal concentrations for the crystallization of RPS4TIR, RRS1TIR and SNC1TIR were determined to be 10, 2 and 5 mg ml^{-1}, respectively. Initial crystallization screening was conducted at 293 K using 200 nl drops in 96-well plates. Crystals of RPS4TIR grew after 1 d in JCSG *plus* condition No. 3 consisting of 0.18 *M* tribasic ammonium citrate, 20%(*w/v*) PEG 3350. After initial optimization experiments in which the precipitant, salt and pH were manipulated, the crystals remained small and fragile. In an attempt to improve the crystal growth and morphology, we used the Additive Screen (Hampton Research). It was observed that the addition of numerous chloride-containing salts greatly improved the crystal morphology, with sodium chloride achieving the best morphological appearance. Long and thin plate-like crystals were obtained using a protein concentration of 10 mg ml^{-1} in a crystallization condition consisting of 23%(*w/v*) PEG 3350, 0.2 *M* ammonium citrate pH 6.5, 0.2 *M* sodium chloride at 293 K (Fig. 1*a*). A data set was collected for RPS4TIR to 2.05 Å resolution (Table 1; Fig. 2*a*). The crystals of RPS4TIR have the symmetry of space group *P*1 and are most likely to contain four molecules in the asymmetric unit, corresponding to a solvent content of 49% as calculated by *MATTHEWS_COEF* (Matthews, 1968; Kantardjieff & Rupp, 2003) within the *CCP*4 suite (Winn *et al.*, 2011).

Crystals of RRS1TIR appeared after 1 d in Index condition No. 4 consisting of 0.2 *M* ammonium sulfate pH 7.5, 0.1 *M* bis-tris pH 6.5. After optimization, tetragonal crystals were obtained in a buffer consisting of 0.1 *M* bis-tris pH 7.0, 1.8 *M* ammonium sulfate using a protein concentration of 2 mg ml^{-1} at 293 K (Fig. 1*b*). A data set was collected at 1.75 Å resolution (Table 1; Fig. 2*b*). The crystals of RRS1TIR have the symmetry of space group $P4_12_12$ or $P4_32_12$ and are most likely to contain one molecule in the asymmetric unit, corresponding to a solvent content of 50% as calculated by *MATTHEWS_COEF* (Matthews, 1968; Kantardjieff & Rupp, 2003) within the *CCP*4 suite (Winn *et al.*, 2011).

The RRS1 TIR domain is an atypical plant TIR domain because it has a shorter αD helical region compared with other plant TIR domains (Fig. 3). AtTIR (Chan *et al.*, 2010) represents the best sequence match for the RRS1 TIR domain to any protein with known structure, with a sequence identity of 21%. In light of the low sequence identity and the deletion within the αD helical region, we were unsure whether molecular replacement (MR) would be suitable for structure determination. To provide additional phase information based on sulfur single-wavelength anomalous diffraction (SAD), another data set was collected from the same crystal at a longer wavelength to maximize the anomalous signal from the S atoms (Table 1; the wavelength was chosen as a compromise to balance radiation damage and maximizing the anomalous signal). There are five S atoms in one molecule of the RRS1 TIR domain contributed by one methionine residue and four cysteine residues. We do not expect that the structure can be solved based solely on sulfur SAD data and intend to solve the structure by a combination of MR and SAD phasing.

The initial crystallization screens for SNC1TIR were set up with a protein concentration of 5 mg ml^{-1}. Crystals of SNC1TIR appeared after 1 d under several different screening conditions with PEG 3350 as precipitant, including Index condition No. 44 consisting of 0.1 *M* HEPES pH 7.5, 37.5%(*w/v*) PEG 3350 and Index condition No. 45 consisting of 0.1 *M* Tris pH 8.5, 37.5%(*w/v*) PEG 3350. Optimization was carried out with PEG 3350 as precipitant and MMT (L-malic acid, MES, Tris) buffer to control the pH (Newman, 2004). The initial crystals were long and needle-like. Thicker orthorhombic crystals were obtained after glycerol was added to the screening solution. The best crystals grew in 18%(*w/v*) PEG 3350, 9%(*w/v*) glycerol, 0.1 *M* MMT buffer pH 7.5 with a protein concentration of 5 mg ml^{-1} at 293 K (Fig. 1*c*). A data set was collected to 2.20 Å resolution (Fig. 2*c*). The crystals of SNC1TIR have the symmetry of space group $P4_12_12$ or $P4_32_12$ and are most likely contain two molecules in the asymmetric unit, corresponding to a solvent content of 53% as calculated by *MATTHEWS_COEF* (Matthews, 1968; Kantardjieff & Rupp, 2003) within the *CCP*4 suite (Winn *et al.*, 2011).

Structure determination of the RPS4, RRS1 and SNC1 TIR domains is currently under way. The crystal structures will provide new insights into the molecular details of the roles of TIR domains during plant immune signalling and in particular any differences between the RPS4/RRS1 dual resistance-protein system compared with the L6 protein. Comparative studies of different R-protein TIR domains will further shed light on the common features of the interfaces involved in TIR–TIR domain interactions.

crystallization communications

References

Ashikawa, I., Hayashi, N., Yamane, H., Kanamori, H., Wu, J., Matsumoto, T., Ono, K. & Yano, M. (2008). *Genetics*, **180**, 2267–2276.

Bernoux, M., Ve, T., Williams, S., Warren, C., Hatters, D., Valkov, E., Zhang, X., Ellis, J. G., Kobe, B. & Dodds, P. N. (2011). *Cell Host Microbe*, **9**, 200–211.

Birker, D., Heidrich, K., Takahara, H., Narusaka, M., Deslandes, L., Narusaka, Y., Reymond, M., Parker, J. E. & O'Connell, R. (2009). *Plant J.* **60**, 602–613.

Chan, S. L., Mukasa, T., Santelli, E., Low, L. Y. & Pascual, J. (2010). *Protein Sci.* **19**, 155–161.

Chisholm, S. T., Coaker, G., Day, B. & Staskawicz, B. J. (2006). *Cell*, **124**, 803–814.

Deslandes, L., Olivier, J., Peeters, N., Feng, D. X., Khounlotham, M., Boucher, C., Somssich, I., Genin, S. & Marco, Y. (2003). *Proc. Natl Acad. Sci. USA*, **100**, 8024–8029.

Deslandes, L., Olivier, J., Theulieres, F., Hirsch, J., Feng, D. X., Bittner-Eddy, P., Beynon, J. & Marco, Y. (2002). *Proc. Natl Acad. Sci. USA*, **99**, 2404–2409.

Dodds, P. N., Lawrence, G. J., Catanzariti, A.-M., Teh, T., Wang, C.-I. A., Ayliffe, M. A., Kobe, B. & Ellis, J. G. (2006). *Proc. Natl Acad. Sci. USA*, **103**, 8888–8893.

Dodds, P. N. & Rathjen, J. P. (2010). *Nature Rev. Genet.* **11**, 539–548.

Edgar, R. C. (2004). *Nucleic Acids Res.* **32**, 1792–1797.

Evans, P. R. & Murshudov, G. N. (2013). *Acta Cryst.* D**69**, 1204–1214.

Gassmann, W., Hinsch, M. E. & Staskawicz, B. J. (1999). *Plant J.* **20**, 265–277.

Gouet, P., Robert, X. & Courcelle, E. (2003). *Nucleic Acids Res.* **31**, 3320–3323.

Jones, J. D. G. & Dangl, J. L. (2006). *Nature (London)*, **444**, 323–329.

Kabsch, W. (2010). *Acta Cryst.* D**66**, 125–132.

Kantardjieff, K. A. & Rupp, B. (2003). *Protein Sci.* **12**, 1865–1871.

Karplus, P. A. & Diederichs, K. (2012). *Science*, **336**, 1030–1033.

Lee, S.-K., Song, M.-Y., Seo, Y.-S., Kim, H.-K., Ko, S., Cao, P.-J., Suh, J.-P., Yi, G., Roh, J.-H., Lee, S., An, G., Hahn, T.-R., Wang, G.-L., Ronald, P. & Jeon, J.-S. (2009). *Genetics*, **181**, 1627–1638.

Li, X., Clarke, J. D., Zhang, Y. & Dong, X. (2001). *Mol. Plant Microbe Interact.* **14**, 1131–1139.

Lukasik, E. & Takken, F. L. (2009). *Curr. Opin. Plant Biol.* **12**, 427–436.

Maekawa, T., Cheng, W., Spiridon, L. N., Töller, A., Lukasik, E., Saijo, Y., Liu, P., Shen, Q.-H., Micluta, M. A., Somssich, I. E., Takken, F. L. W., Petrescu, A. J., Chai, J. & Schulze-Lefert, P. (2011). *Cell Host Microbe*, **9**, 187–199.

Matthews, B. W. (1968). *J. Mol. Biol.* **33**, 491–497.

McPhillips, T. M., McPhillips, S. E., Chiu, H.-J., Cohen, A. E., Deacon, A. M., Ellis, P. J., Garman, E., Gonzalez, A., Sauter, N. K., Phizackerley, R. P., Soltis, S. M. & Kuhn, P. (2002). *J. Synchrotron Rad.* **9**, 401–406.

Narusaka, M., Kubo, Y., Shiraishi, T., Iwabuchi, M. & Narusaka, Y. (2009). *Plant Signal. Behav.* **4**, 954–955.

Narusaka, M., Shirasu, K., Noutoshi, Y., Kubo, Y., Shiraishi, T., Iwabuchi, M. & Narusaka, Y. (2009). *Plant J.* **60**, 218–226.

Newman, J. (2004). *Acta Cryst.* D**60**, 610–612.

Okuyama, Y., Kanzaki, H., Abe, A., Yoshida, K., Tamiru, M., Saitoh, H., Fujibe, T., Matsumura, H., Shenton, M., Galam, D. C., Undan, J., Ito, A., Sone, T. & Terauchi, R. (2011). *Plant J.* **66**, 467–479.

Padmanabhan, M., Cournoyer, P. & Dinesh-Kumar, S. P. (2009). *Cell. Microbiol.* **11**, 191–198.

Ravensdale, M., Bernoux, M., Ve, T., Kobe, B., Thrall, P. H., Ellis, J. G. & Dodds, P. N. (2012). *PLoS Pathog.* **8**, e1003004.

Sinapidou, E., Williams, K., Nott, L., Bahkt, S., Tör, M., Crute, I., Bittner-Eddy, P. & Beynon, J. (2004). *Plant J.* **38**, 898–909.

Stols, L., Gu, M., Dieckman, L., Raffen, R., Collart, F. R. & Donnelly, M. I. (2002). *Protein Expr. Purif.* **25**, 8–15.

Studier, F. W. (2005). *Protein Expr. Purif.* **41**, 207–234.

Wang, C.-I. A., Gunčar, G., Forwood, J. K., Teh, T., Catanzariti, A.-M., Lawrence, G. J., Loughlin, F. E., Mackay, J. P., Schirra, H. J., Anderson, P. A., Ellis, J. G., Dodds, P. N. & Kobe, B. (2007). *Plant Cell*, **19**, 2898–2912.

Williams, S. J., Sornaraj, P., deCourcy-Ireland, E., Menz, R. I., Kobe, B., Ellis, J. G., Dodds, P. N. & Anderson, P. A. (2011). *Mol. Plant Microbe Interact.* **24**, 897–906.

Winn, M. D. *et al.* (2011). *Acta Cryst.* D**67**, 235–242.

Wirthmueller, L., Zhang, Y., Jones, J. D. G. & Parker, J. E. (2007). *Curr. Biol.* **17**, 2023–2029.

Yuan, B., Zhai, C., Wang, W., Zeng, X., Xu, X., Hu, H., Lin, F., Wang, L. & Pan, Q. (2011). *Theor. Appl. Genet.* **122**, 1017–1028.

Zhu, Z., Xu, F., Zhang, Y., Cheng, Y. T., Wiermer, M., Li, X. & Zhang, Y. (2010). *Proc. Natl Acad. Sci. USA*, **107**, 13960–13965.